Supplement of

Technical note: Influence of different averaging metrics and temporal resolutions on aerosol pH calculated by thermodynamic modeling

5   Haoqi Wang[1,2,★], Xiao Tian[1,2,★], Wanting Zhao[1,2], Jiacheng Li[1,2], Haoyu Yu[1], Yinchang Feng[1,2], Shaojie Song[1,2]

[1]State Environmental Protection Key Laboratory of Urban Ambient Air Particulate Matter Pollution Prevention and Control, College of Environmental Science and Engineering, Nankai University, Tianjin 300350, China

[2]CMA-NKU Cooperative Laboratory for Atmospheric Environment-Health Research, Tianjin 300350, China

10   [★]These authors contributed equally to this work.

Correspondence to: Shaojie Song (songs@nankai.edu.cn)

- Texts S1−S2
15
- Figures S1−S4
- Tables S1−S3

Text S1. Settings for the GEOS-Chem chemical transport model simulations

Emission databases were prepared using the Harvard-NASA Emissions Component (HEMCO, version 3.6.2, DOI: 10.5281/zenodo.7692950) as detailed in the work by Lin et al. (2021). Global anthropogenic emissions were obtained from the Community Emissions Data System (CEDS) for SO_2, NO_x, NH_3, CO, VOCs, dust, primary organic carbon, and black carbon (Hoesly et al., 2018). Subsequently, the Multi-resolution Emission Inventory (MEIC, http://meicmodel.org.cn) covered mainland China (Li et al., 2017; Zheng et al., 2018). Previous studies indicated that bottom-up emission inventories may underestimate NH_3 emissions in northern China by approximately 40% (Zhang et al., 2018; Wang et al., 2018; Kong et al., 2019; Ruan et al., 2022). Hence, NH_3 emissions for the North China Pain region were multiplied by a factor of 1.4. Biogenic VOC emissions were calculated using the Model of Emissions of Gases and Aerosols from Nature (MEGAN, version 2.1) (Guenther et al., 2012). Biomass burning emissions were obtained from the Global Fire Emissions Database (GFED4, version 4.1) (Van Der Werf et al., 2017). Other emissions included volcanic SO_2 sources (Ge et al., 2016), lightning and soil NO_x sources (Murray et al., 2012; Hudman et al., 2012), mineral dust emissions (Duncan et al., 2007), and natural NH_3 sources (https://www.geiacenter.org, last accessed 2024-02-16). The tropospheric chemistry mechanism encompassed detailed reactions for ozone–NOx–VOC–aerosol–halogen interactions. The parameterization scheme for the heterogeneous uptake of sulfate in KPP was referred to Wang et al. (2014) and Wang et al. (2021). Similar to earlier studies (Wang et al., 2024), an apparent reactive uptake coefficient for SO_2 was adopted to compensate for the underestimate of sulfate during the North China winter season, and the reactive uptake coefficient (γ) was taken as 10^{-4} at RH > 50%. Gaseous and particle dry deposition adhered to a conventional resistance-in-series scheme (Wesely, 1989). Wet deposition encompassed in-cloud scavenging, below-cloud scavenging, and scavenging within convective updrafts (Amos et al., 2012).

Text S2. Theoretical calculations based on the multiphase buffer theory

Based on the multiphase buffer theory (Zheng et al., 2020), for gas-liquid multiphase systems, pH becomes a function of K_a^*

40   and the ratio of total NH_3 in both gas and aqueous phase to NH_4^+ in the aqueous phase.

$$pH = pK_{a,NH_3}^* + \log_{10} \frac{[NH_3(aq)] + [NH_3(g)]}{\left[a_{NH_4^+(aq)}\right]}$$

where

$$K_{a,NH_3}^* = \frac{[H^+(aq)]([NH_3(aq)]+[NH_3(g)])}{\left[a_{NH_4^+(aq)}\right]} = K_{a,NH_3}\left(1 + \frac{1}{H_{NH_3}RTAWC}\right)$$

$$H_{NH_3} = \frac{\left[a_{NH_4^+(aq)}\right]}{p_{NH_3}} = \frac{1}{RTAWC}\frac{\left[a_{NH_4^+(aq)}\right]}{[NH_3(g)]}$$

45

$$[NH_3(g)] = \frac{p_{NH_3}}{RTAWC}$$

$$\left[a_{NH_4^+(aq)}\right] = [NH_4^+(aq)]\gamma_{NH_4^+(aq)}$$

$[NH_3(aq)]$ represents the molality of NH_3 in aerosol liquid water (mol kg^{-1} water). $[NH_3(g)]$ is an introduced parameter to represent the equivalent molality of gaseous NH_3 in aerosol liquid water (mol kg^{-1} water). $[NH_4^+(aq)]$ is the molality of NH_4^+ in aerosol liquid water (mol kg^{-1} water). $\left[a_{NH_4^+(aq)}\right]$ is the activity of NH_4^+ in aerosol liquid water (mol kg^{-1} water). K_{a,NH_3} is

50   the molality-based equilibrium constant for the acid dissociation of NH_4^+ (mol kg^{-1}). H_{NH_3} is Henry's law constant of NH_3 in mol kg^{-1} atm^{-1} (57.64 mol kg^{-1} atm^{-1} at 298.15 K, 208.02 mol kg^{-1} atm^{-1} at 273.15 K). R is the gas constant (0.08205 atm L mol^{-1} K^{-1}). T is temperature in K. AWC is the aerosol water content (μg m^{-3} air). p_{NH_3} is partial pressure of NH_3 (atm). $c_{NH_4^+(aq)}$ is the mass concentration of NH_3 in the atmosphere (μg m^{-3} air). $\gamma_{NH_4^+(aq)}$ is the activity coefficient (unitless).

Taking K_{a,NH_3}^*, and H_{NH_3} into the calculation of pH, the formula can be simplified as follows:

55    $$pH = pK_{a,NH_3}^* + \log_{10}\frac{[NH_3(aq)] + [NH_3(g)]}{\left[a_{NH_4^+(aq)}\right]}$$

$$= -\log_{10}\left(K_{a,NH_3}\frac{H_{NH_3}RTAWC + 1}{H_{NH_3}RTAWC}\right) + \log_{10}\left(\frac{[NH_3(g)]\left(H_{NH_3}RTAWC + 1\right)}{\left[a_{NH_4^+(aq)}\right]}\right)$$

$$= \log_{10}\left(\frac{[NH_3(g)]AWC}{\left[a_{NH_4^+(aq)}\right]}\frac{H_{NH_3}RT}{K_{a,NH_3}}\right)$$

$$= \log_{10}\left(\frac{p_{NH_3}}{[NH_4^+(aq)]\gamma_{NH_4^+(aq)}}\frac{H_{NH_3}}{K_{a,NH_3}}\right)$$

$$= \log_{10}\left(\frac{p_{NH_3}}{[NH_4^+(aq)]\gamma_{NH_4^+(aq)}}\right) + C_T$$

60     $C_T = \log_{10}\left(\frac{H_{NH_3}}{K_{a,NH_3}}\right)$ can be simplified as a constant given the limited temperature variation in winter in the North China Plain.

Ultimately, pH can be considered as a function of p_{NH_3}, $[NH_4^+(aq)]$, and $\gamma_{NH_4^+(aq)}$.
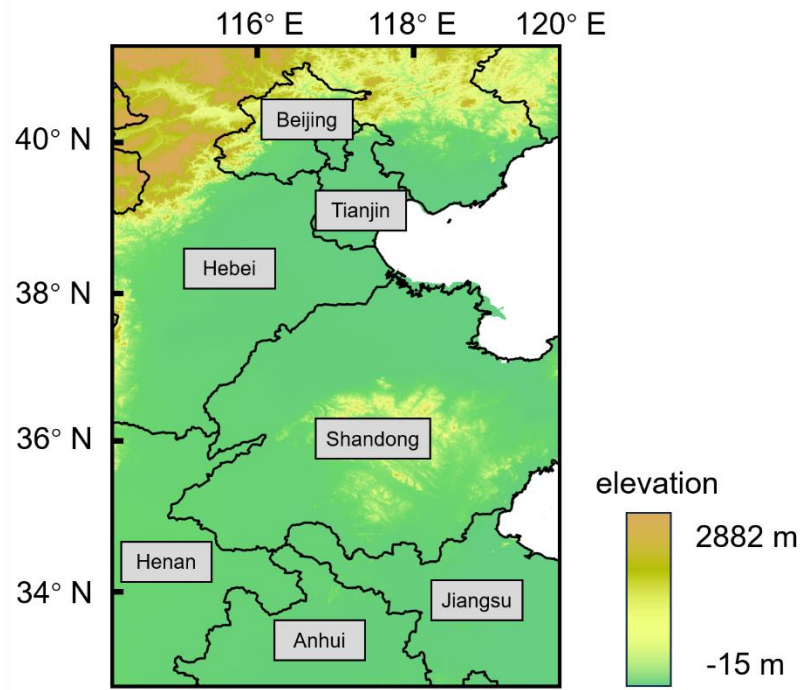
Figure S1. Topographic map of the study region. The North China Plain is situated in northern China and spans a latitude and longitude range of 33°N−41°N, 114.375°E−120°E in the GEOS-Chem model domain, covering a total of 162 grids horizontally.
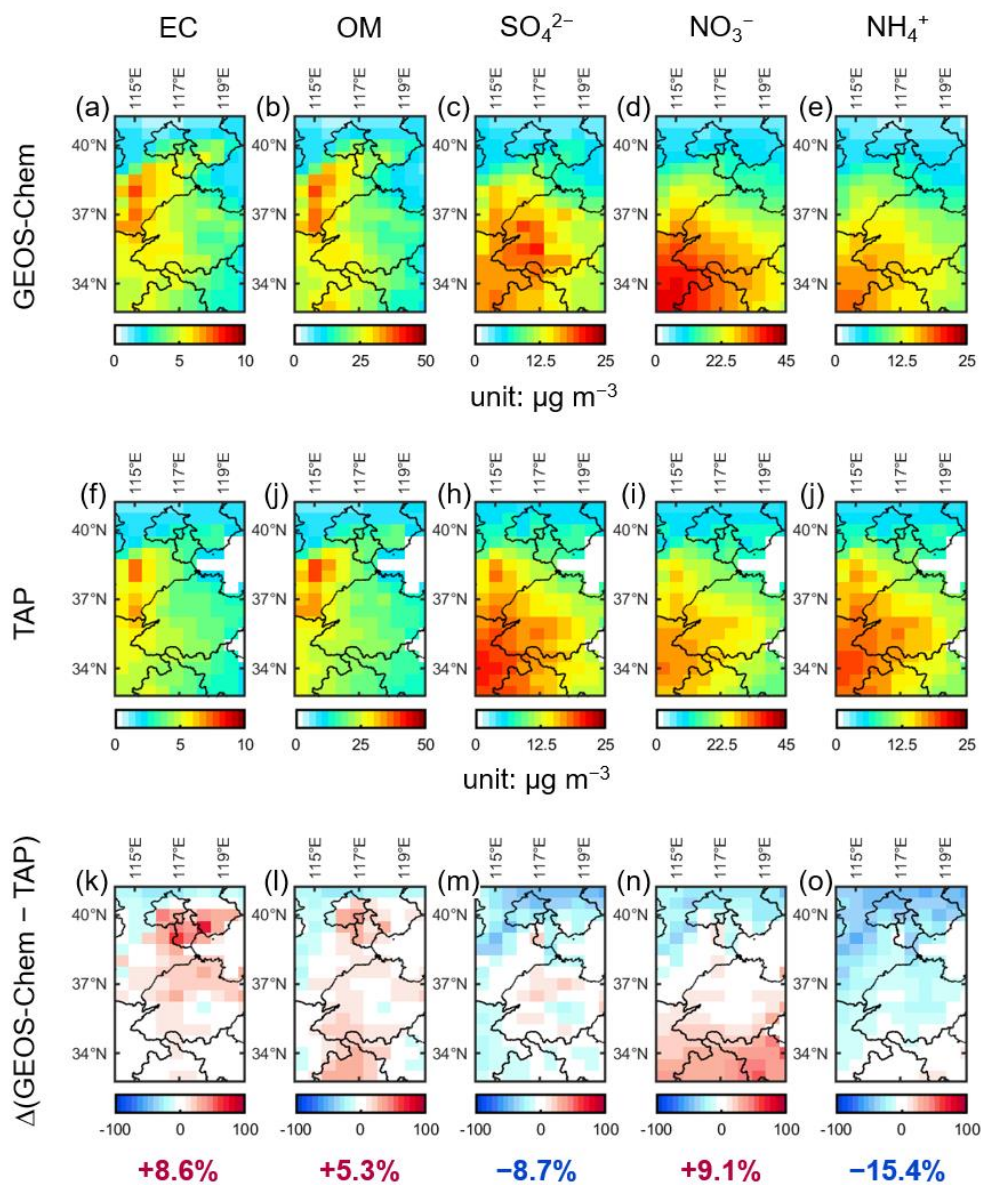
Figure S2. Evaluation of the GEOS-Chem chemical transport model simulation during winter 2018 using the TAP reanalysis data product. EC (elemental carbon), OM (organic material), SO_4^-, NO_3^-, and NH_4^+ (corresponding to the first through fifth columns, respectively) were chosen as validation species. The first row displayed the GEOS-Chem simulations ($\mu g\ m^{-3}$). The second row represented the concentration from TAP ($\mu g\ m^{-3}$), serving as a standard for comparison. The third row presented the percentage of relative difference (%), where positive and negative values indicated model overestimation and underestimation, respectively.
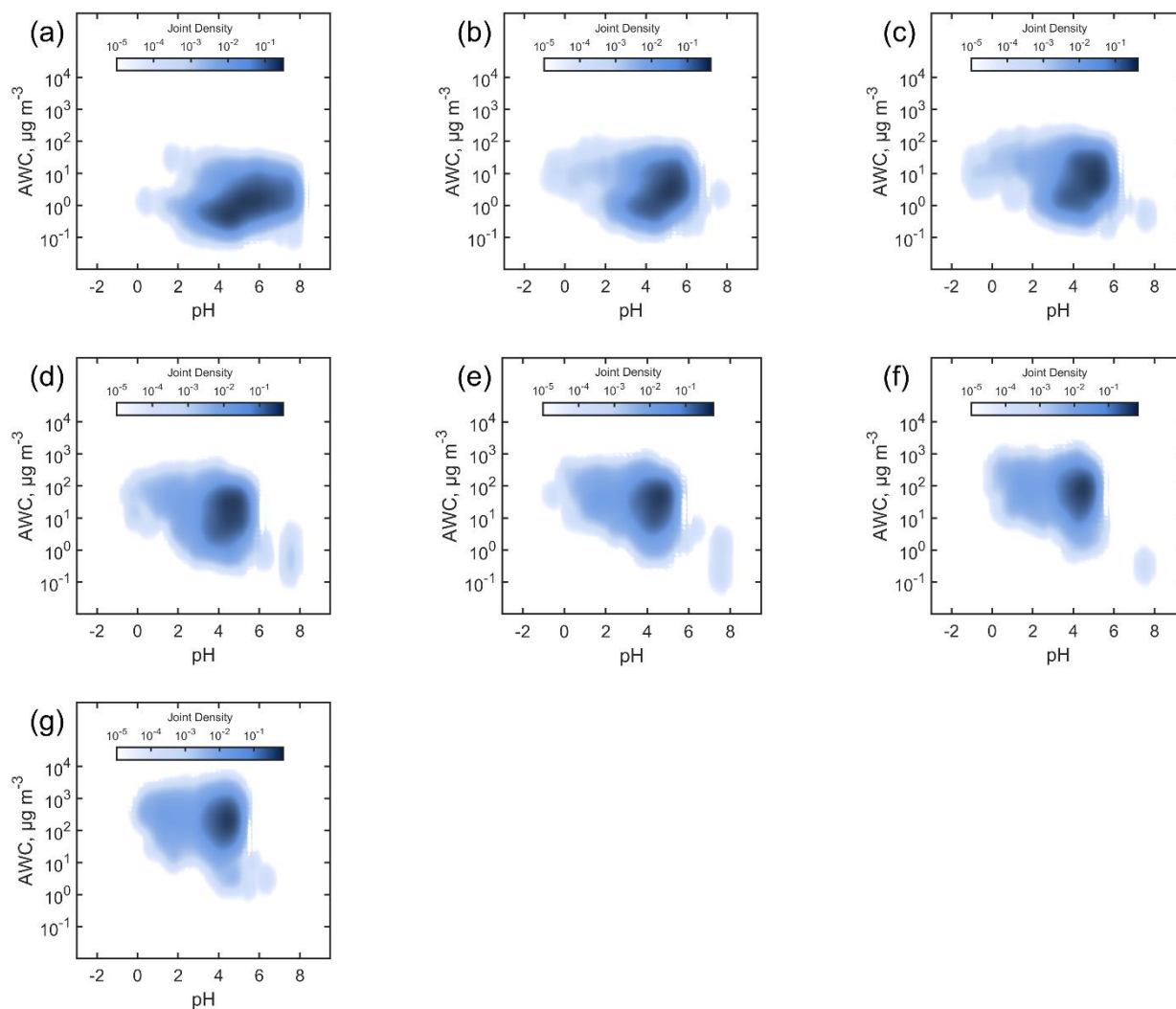
Figure S3. (a) Probability distributions of the joint probability distribution of AWC and aerosol pH for RH between 25% and 35%. (b-g) are the same as (a), but the RH ranges from 35% to 95% in 10% intervals.
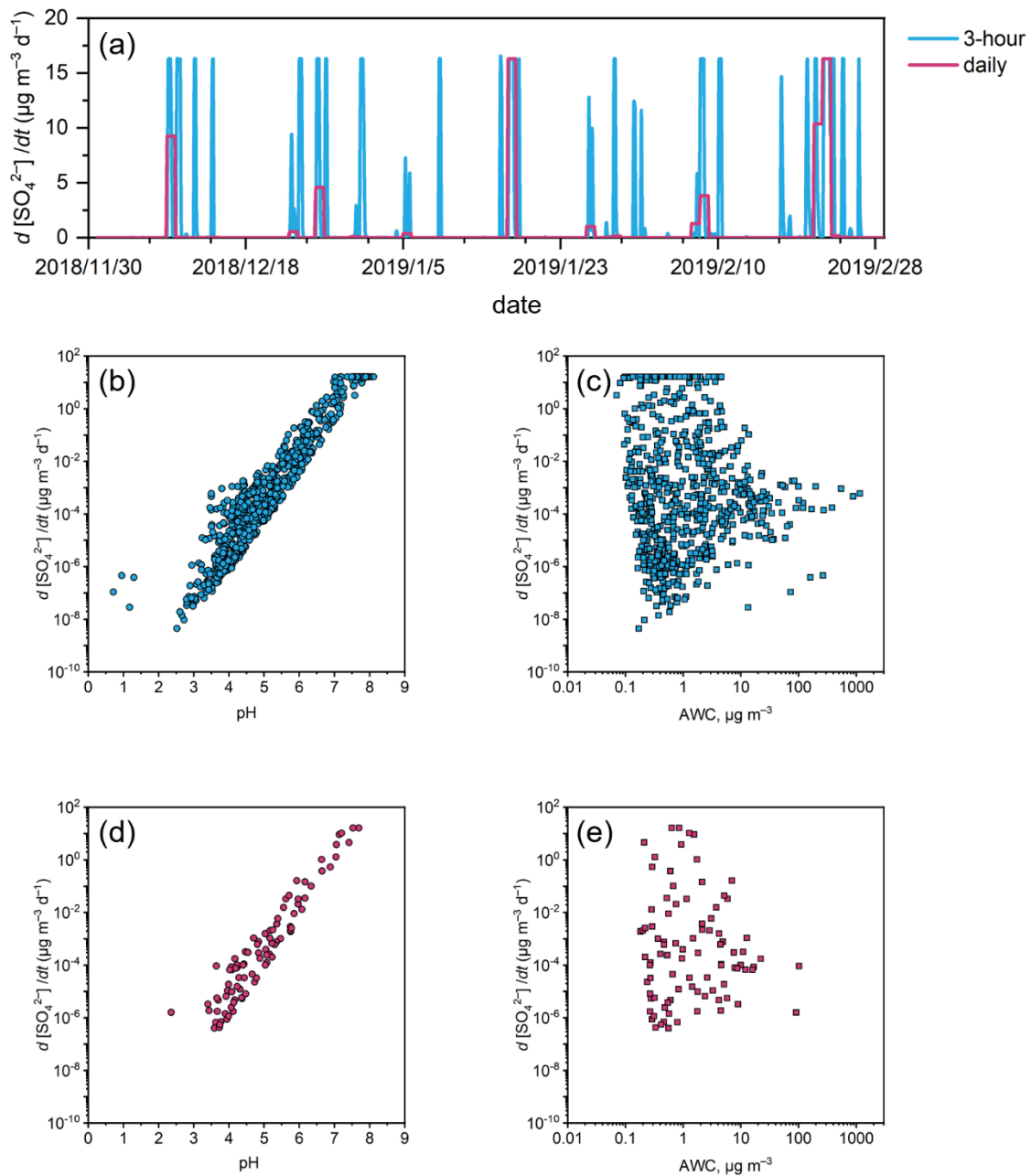
Figure S4. (a) Comparison of the trends in sulfate formation rates based on 3-hour (blue line) and daily (pink line) resolution data; (b) d(SO_4^{2-})/dt vs. pH and (c) d(SO_4^{2-})/dt vs. AWC based on 3-hour resolution data; (d) d(SO_4^{2-})/dt vs. pH and (e) d(SO_4^{2-})/dt vs. AWC based on daily resolution data.

Table S1. Reported aerosol pH from thermodynamic modeling based on chemical transport model simulation data and field observational data

Area	Period	Data sources	Average metric	Time resolution	Average pH	Reference
			Chemical transport model simulation data			
U.S.	2050 [a]	WRF-CMAQ	$\overline{pH}$* [b]	hourly, daily	1.8	Chen et al. (2019)
U.S.	2011	WRF-CMAQ	$\overline{pH}$	not clear	1.8 ± 0.5	Zhang et al. (2021)
Eastern U.S.	2001	WRF-CMAQ	pH	annual	1.6	Vasilakos et al. (2018)
	2011				2.5	
Midwestern U.S.	2001 and 2011	WRF-CMAQ	$\overline{pH}$	seasonal	3.5 − 4.0	Lawal et al. (2018)
Southeastern U.S.					1.5 − 2.0	
North China Plain, China	2011	WRF-CMAQ	$\overline{pH}$	not clear	3.8 ± 0.2	Zhang et al. (2021)
Beijing, China	Jan 2013	WRF-Chem	not clear	hourly	5.4	Tao et al. (2020)
North China Plain, China	Oct−Nov 2014	WRF-Chem [c]	$\overline{pH}_w^*$	not clear	2.3 ± 0.4	Ruan et al. (2022)
			Field observational data			
U.S.	2011		$\overline{pH}$	weekly	2.7 ± 0.8	Zhang et al. (2021)
Centerville, U.S.	2008−2015		$\overline{pH}$	seasonal	0.7	Lawal et al. (2018)
				monthly	0.2	
Southeast U.S.	May−Dec 2012		$\overline{pH}$	hourly	0.9 ± 0.6	Guo et al. (2015)
California, U.S.	May−Jun 2010		$\overline{pH}$	hourly	1.9 ± 0.5 (PM$_1$)	Guo et al. (2017)
					2.7 ± 0.3 (PM$_{2.5}$)	
Georgia, U.S.	Autumn 2016		$\overline{pH}$	hourly	2.2 ± 0.6 (PM$_1$)	Nah et al. (2018)
Mexico City, Mexico	Mar-Apr 2006		$\overline{pH}$	10 min	3.3	Hennigan et al. (2015)
Finokalia, Greece	Aug−Nov 2012		$\overline{pH}$	30 min	1.3 ± 1.1 (PM$_1$)	Bougiatioti et al. (2016)
Veneto, Greece	Dec 2012−Feb 2013		$\overline{pH}$	daily	3.9 ± 0.3	Masiol et al. (2020)
	Jun−Aug 2012				2.2 ± 0.3	
Seoul, South Korea	May−Jun 2016		$\overline{pH}$	hourly	2.5 ± 0.7	Kim et al. (2022)
Indo-Gangetic Plain, India	Summer 2018		$\overline{pH}$	daily	2.9 ± 0.7	Sharma et al. (2022)
	Autumn 2018				2.7 ± 0.2	
	Winter 2018				3.2 ± 0.3	
Indo-Gangetic Plain, India	Winter 2017		$\overline{pH}$	hourly	4.5 ± 0.5 (PM$_1$)	Acharja et al. (2023)
					4.6 ± 0.5 (PM$_{2.5}$)	
Beijing, China	Winter 2015−2016		not clear	hourly	4.2	Liu et al. (2017)
Beijing, China	Dec 2016		$\overline{pH}$	hourly	5.6 ± 0.8	Meng et al. (2020)
Beijing, China	Spring 2016		$\overline{pH}$	hourly	4.4 ± 1.2	Ding et al. (2019)
	Summer 2017				4.5 ± 0.7	
	Autumn 2017				3.8 ± 1.2	
	Winter 2017				4.3 ± 0.8	
Tianjin, China	Dec 2024−Jun 2015		$\overline{pH}$	hourly	4.9 ± 1.4	Shi et al. (2017)
Gucheng, China	Winter 2016		not clear	daily	5.3	Chi et al. (2018)
Zhengzhou, China	Winter 2019		$\overline{pH}$	hourly	4.4 ± 1.5	Jiang et al. (2022)
Shanghai, China	Feb 2012		$\overline{pH}$	hourly	2.9 (haze)	Kong et al. (2018)
					3.1 (clean)	
Shanghai, China	Spring 2011−2019		$\overline{pH}$	hourly	3.3 ± 0.5	Zhou et al. (2022)
	Summer 2011−2019				2.9 ± 0.5	
	Autumn 2011−2019				3.0 ± 0.5	
	Winter 2011−2019				3.6 ± 0.6	

Shanghai, China	Spring 2019−2020	$\overline{pH}$	hourly	3.1 ± 0.5	Fu et al. (2022)
	Summer 2019−2020			2.6 ± 0.5	
	Autumn 2019−2020			2.7 ± 0.6	
	Winter 2019−2020			3.5 ± 0.4	
Guangzhou, China	Nov 2012−Oct 2013	$\overline{pH}$	hourly	2.5 ± 0.7	Jia et al. (2020)
Shenzhen, China	Sep−Oct 2019	$\overline{pH}$	hourly	1.6 ± 0.5	Wang et al. (2022)

85   Unless noted, the thermodynamic models used in this table are ISORROPIA-II with the forward mode (using total (gas plus aerosol phase) concentrations as model

inputs) assumption.

[a] The 2050 emissions were estimated from a future baseline scenario based on the RCP4.5 pathway.

[b] Daily average aerosol pH values were calculated using daily average equilibrium H^+ concentrations and AWC based on the CMAQ hourly output. Annual average

aerosol pH was then calculated by averaging the daily aerosol pH.

90   [c] WRF-Chem used the MOSAIC thermodynamic scheme to predict aerosol pH.

Table S2. Rate expression and rate coefficients of aqueous-phase reaction of SO_2 oxidation by O_3

Oxidants	Rate Expression, -d[S(IV)]/dt	Reference
O_3	$(k_0[SO_2 \cdot H_2O] + k_1[HSO_3^-] + k_2[SO_3^{2-}])[O_3(aq)]$	Cheng et al. (2016)
	$k_0 = 2.4 \times 10^4\ M^{-1}\ s^{-1}$	
	$k_1 = 3.7 \times 10^5\ M^{-1}\ s^{-1}$, E/R = 5530 K[a]	
	$k_2 = 1.5 \times 10^9\ M^{-1}\ s^{-1}$, E/R = 5280 K[a]	

[a] According to the Arrhenius equation, the relationship between the kinetic constant k and the temperature T can be expressed as $k(T) = k(T_0) \exp[-\frac{E}{R}(\frac{1}{T} - \frac{1}{T_0})]$, where

T_0 = 298 K.

95

$(k_0[SO_2 \cdot H_2O] + k_1[HSO_3^-] + k_2[SO_3^{2-}])[O_3(aq)]$

$k_0 = 2.4 \times 10^4\ M^{-1}\ s^{-1}$

$k_1 = 3.7 \times 10^5\ M^{-1}\ s^{-1}$, E/R = 5530 K[a]

$k_2 = 1.5 \times 10^9\ M^{-1}\ s^{-1}$, E/R = 5280 K[a]

Table S3. The calculation of the apparent Henry's constant (H^*)

Gas-Aqueous Equilibrium for S(IV)			
Equilibrium	Constant Symbol	H_{298K} (M atm^{-1})[a]	$-\Delta H_{298K}/R$(K)
$SO_2(g) \leftrightarrow SO_2(aq)$	H_{SO2}	1.23	3145.3
$O_3(g) \leftrightarrow O_3(aq)$	H_{O3}	1.1×10^{-2}	2536.4
Aqueous-phase Ionization Equilibrium [b]			
Equilibrium	Constant Symbol	H_{298K} (M atm^{-1})[a]	$-\Delta H_{298K}/R$(K)
$SO_2 \cdot H_2O \leftrightarrow H^+ + HSO_3^-$	K_{S1}	1.3×10^{-2}	1960
$HSO_3^- \leftrightarrow H^+ + SO_3^{2-}$	K_{S2}	6.6×10^{-8}	1500

[a] The Henry's constant (H) and ionization constant (K) both demonstrate a similar temperature dependence. The H at temperature T is $H(T) = H(T_0) \exp[-\frac{\Delta H_{298K}}{R}(\frac{1}{T} - \frac{1}{T_0})]$, where $T_0 = 298$ K. The same is true for K(T).

[b] The effective Henry's constant (H^*) for HSO_3^- and SO_3^{2-} are respectively

$$H^*_{HSO_3^-} = H_{SO_2} \frac{K_{S1}}{[H^+]}$$

$$H^*_{SO_3^{2-}} = H_{SO_2} \frac{K_{S1}K_{S2}}{[H^+]^2}$$

where H_{SO_2}, K_{S1}, and K_{S2} are corresponding values at temperature T.

100

References

105   Acharja, P., Ghude, S., Sinha, B., Barth, M., Govardhan, G., Kulkarni, R., Sinha, V., Kumar, R., Ali, K., Gultepe, I., Petit, J. E., and Rajeevan, M.: Thermodynamical framework for effective mitigation of high aerosol loading in the Indo-Gangetic Plain during winter, Sci. Rep., 13, 13667, 10.1038/s41598-023-40657-w, 2023.

Amos, H. M., Jacob, D. J., Holmes, C. D., Fisher, J. A., Wang, Q., Yantosca, R. M., Corbitt, E. S., Galarneau, E., Rutter, A. P., Gustin, M. S., Steffen, A., Schauer, J. J., Graydon, J. A., Louis, V. L. S., Talbot, R. W., Edgerton, E. S., Zhang, Y.,

110   and Sunderland, E. M.: Gas-particle partitioning of atmospheric Hg(II) and its effect on global mercury deposition, Atmos. Chem. Phys., 12, 591-603, 10.5194/acp-12-591-2012, 2012.

Bougiatioti, A., Nikolaou, P., Stavroulas, I., Kouvarakis, G., Weber, R., Nenes, A., Kanakidou, M., and Mihalopoulos, N.: Particle water and pH in the eastern Mediterranean: source variability and implications for nutrient availability, Atmos. Chem. Phys., 16, 4579-4591, 10.5194/acp-16-4579-2016, 2016.

115   Chen, Y., Shen, H., and Russell, A.: Current and Future Responses of Aerosol pH and Composition in the U.S. to Declining SO2 Emissions and Increasing NH3 Emissions, Environ. Sci. Technol., 53, 9646-9655, 10.1021/acs.est.9b02005, 2019.

Cheng, Y., Zheng, G., Wei, C., Mu, Q., Zheng, B., Wang, Z., Gao, M., Zhang, Q., He, K., Carmichael, G., Pöschl, U., and Su, H.: Reactive nitrogen chemistry in aerosol water as a source of sulfate during haze events in China, Sci. Adv., 2, e1601530, 10.1126/sciadv.1601530, 2016.

120   Chi, X., He, P., Jiang, Z., Yu, X., Yue, F., Wang, L., Li, B., Kang, H., Liu, C., and Xie, Z.: Acidity of Aerosols during Winter Heavy Haze Events in Beijing and Gucheng, China, J. Meteorol. Res., 32, 14-25, 10.1007/s13351-018-7063-4, 2018.

Ding, J., Zhao, P., Su, J., Dong, Q., Du, X., and Zhang, Y.: Aerosol pH and its driving factors in Beijing, Atmos. Chem. Phys., 19, 7939-7954, 10.5194/acp-19-7939-2019, 2019.

Duncan, F. T., Jacob, D. J., and Park, R. J.: The impact of transpacific transport of mineral dust in the United States,

125   Atmospheric Environ., 41, 1251-1266, 10.1016/j.atmosenv.2006.09.048, 2007.

Fu, Z., Cheng, L., Ye, X., Ma, Z., Wang, R., Duan, Y. S., Juntao, H., and Chen, J.: Characteristics of aerosol chemistry and acidity in Shanghai after PM2.5 satisfied national guideline: Insight into future emission control, Sci. Total Environ., 827, 154319, 10.1016/j.scitotenv.2022.154319, 2022.

Ge, C., Wang, J., Carn, S., Yang, K., Ginoux, P., and Krotkov, N.: Satellite-based global volcanic SO₂ emissions and sulfate

130   direct radiative forcing during 2005–2012, J. Geophys. Res.-Atmos, 121, 3446-3464, 10.1002/2015JD023134, 2016.

Guenther, A. B., Jiang, X., Heald, C. L., Sakulyanontvittaya, T., Duhl, T., Emmons, L. K., and Wang, X.: The Model of Emissions of Gases and Aerosols from Nature version 2.1 (MEGAN2.1): an extended and updated framework for modeling biogenic emissions, Geosci. Model Dev., 5, 1471-1492, 10.5194/gmd-5-1471-2012, 2012.

Guo, H., Liu, J., Froyd, K. D., Roberts, J. M., Veres, P. R., Hayes, P. L., Jimenez, J. L., Nenes, A., and Weber, R. J.: Fine

135   particle pH and gas–particle phase partitioning of inorganic species in Pasadena, California, during the 2010 CalNex campaign, Atmos. Chem. Phys., 17, 5703-5719, 10.5194/acp-17-5703-2017, 2017.

Guo, H., Xu, L., Bougiatioti, A., Cerully, K. M., Capps, S. L., Hite Jr, J. R., Carlton, A. G., Lee, S. H., Bergin, M. H., Ng, N. L., Nenes, A., and Weber, R. J.: Fine-particle water and pH in the southeastern United States, Atmos. Chem. Phys., 15, 5211-5228, 10.5194/acp-15-5211-2015, 2015.

140   Hennigan, C. J., Izumi, J., Sullivan, A. P., Weber, R. J., and Nenes, A.: A critical evaluation of proxy methods used to estimate the acidity of atmospheric particles, Atmos. Chem. Phys., 15, 2775-2790, 10.5194/acp-15-2775-2015, 2015.

Hoesly, R. M., Smith, S. J., Feng, L. Y., Klimont, Z., Janssens-Maenhout, G., Pitkanen, T., Seibert, J. J., Vu, L., Andres, R. J., Bolt, R. M., Bond, T. C., Dawidowski, L., Kholod, N., Kurokawa, J., Li, M., Liu, L., Lu, Z. F., Moura, M. C. P., O'Rourke, P. R., and Zhang, Q.: Historical (1750-2014) anthropogenic emissions of reactive gases and aerosols from the

145   Community Emissions Data System (CEDS), Geosci. Model Dev., 11, 369-408, 10.5194/gmd-11-369-2018, 2018.

Hudman, R. C., Moore, N. E., Mebust, A. K., Martin, R. V., Russell, A. R., Valin, L. C., and Cohen, R. C.: Steps towards a mechanistic model of global soil nitric oxide emissions: implementation and space based-constraints, Atmos. Chem. Phys., 12, 7779-7795, 10.5194/acp-12-7779-2012, 2012.

Jia, S., Chen, W., Zhang, Q., Krishnan, P., Mao, J., Zhong, B., Huang, M., Fan, Q., Zhang, J., Chang, M., Yang, L., and

150   Wang, X.: A quantitative analysis of the driving factors affecting seasonal variation of aerosol pH in Guangzhou, China, Sci. Total Environ., 725, 138228, 10.1016/j.scitotenv.2020.138228, 2020.

Jiang, N., Wei, Y., Zhang, R., Hao, Q., Hao, X., Zhang, C., and Hu, R.: Modeling of reducing NH4NO3 in PM2.5 under high ammonia emission in urban areas: Based on high-resolution data, J. Clean. Prod., 350, 131499, 10.1016/j.jclepro.2022.131499, 2022.

155   Kim, Y., Park, O., Park, S. H., Kim, M. J., Kim, J. Y., Choi, J., Lee, D., Cho, S., and Shim, S.: PM2.5 pH estimation in Seoul during the KORUS-AQ campaign using different thermodynamic models, Atmospheric Environ., 268, 118787, 10.1016/j.atmosenv.2021.118787, 2022.

Kong, L., Du, C., Zhanzakova, A., Cheng, T., Yang, X., Wang, L., Fu, H., Chen, J., and Zhang, S.: Trends in heterogeneous aqueous reaction in continuous haze episodes in suburban Shanghai: An in-depth case study, Sci. Total Environ., 634,
160   1192-1204, 10.1016/j.scitotenv.2018.04.086, 2018.

Kong, L., Tang, X., Zhu, J., Wang, Z., Pan, Y., Wu, H., Wu, L., Wu, Q., He, Y., Tian, S. L., Xie, Y., Liu, Z. R., Sui, W., Han, L., and Carmichael, G.: Improved Inversion of Monthly Ammonia Emissions in China Based on the Chinese Ammonia Monitoring Network and Ensemble Kalman Filter, Environ. Sci. Technol., 53, 12529-12538, 10.1021/acs.est.9b02701, 2019.

165   Lawal, A., Guan, X., Liu, C., Henneman, L. R. F., Vasilakos, P., Bhogineni, V., Weber, R., Nenes, A., and Russell, A.: Linked Response of Aerosol Acidity and Ammonia to SO2 and NOx Emissions Reductions in the United States, Environ. Sci. Technol., 52, 9861-9873, 10.1021/acs.est.8b00711, 2018.

Li, M., Zhang, Q., Kurokawa, J., Woo, J. H., He, K. B., Lu, Z. F., Ohara, T., Song, Y., Streets, D. G., Carmichael, G. R., Cheng, Y. F., Hong, C. P., Huo, H., Jiang, X. J., Kang, S. C., Liu, F., Su, H., and Zheng, B.: MIX: a mosaic Asian
170   anthropogenic emission inventory under the international collaboration framework of the MICS-Asia and HTAP, Atmos. Chem. Phys., 17, 935-963, 10.5194/acp-17-935-2017, 2017.

Lin, H., Jacob, D. J., Lundgren, E. W., Sulprizio, M. P., Keller, C. A., Fritz, T. M., Eastham, S. D., Emmons, L. K., Campbell, P. C., Baker, B., Saylor, R. D., and Montuoro, R.: Harmonized Emissions Component (HEMCO) 3.0 as a versatile emissions component for atmospheric models: application in the GEOS-Chem, NASA GEOS, WRF-GC, CESM2,
175   NOAA GEFS-Aerosol, and NOAA UFS models, Geosci. Model Dev., 14, 5487-5506, 10.5194/gmd-14-5487-2021, 2021.

Liu, M., Song, Y., Zhou, T., Xu, Z., Yan, C., Zheng, M., Wu, Z., Hu, M., Wu, Y., and Zhu, T.: Fine particle pH during severe haze episodes in northern China, Geophys. Res. Lett.,, 44, 5213-5221, 10.1002/2017GL073210, 2017.

Masiol, M., Squizzato, S., Formenton, G., Khan, M. B., Hopke, P. K., Nenes, A., Pandis, S. N., Tositti, L., Benetello, F.,
180   Visin, F., and Pavoni, B.: Hybrid multiple-site mass closure and source apportionment of PM2.5 and aerosol acidity at major cities in the Po Valley, Sci. Total Environ., 704, 135287, 10.1016/j.scitotenv.2019.135287, 2020.

Meng, Z., Wu, L., Xu, X., Xu, W., Zhang, R., Jia, X., Liang, L., Miao, Y., Cheng, H. F., Xie, Y., He, J., and Zhong, J. T.: Changes in ammonia and its effects on PM2.5 chemical property in three winter seasons in Beijing, China, Sci. Total Environ., 749, 142208, 10.1016/j.scitotenv.2020.142208, 2020.

185   Murray, L. T., Jacob, D. J., Logan, J. A., Hudman, R. C., and Koshak, W. J.: Optimized regional and interannual variability of lightning in a global chemical transport model constrained by LIS/OTD satellite data, J. Geophys. Res.-Atmos, 117, D20307, 10.1029/2012JD017934, 2012.

Nah, T., Guo, H., Sullivan, A. P., Chen, Y., Tanner, D. J., Nenes, A., Russell, A., Ng, N. L., Huey, L. G., and Weber, R. J.: Characterization of aerosol composition, aerosol acidity, and organic acid partitioning at an agriculturally intensive rural
190   southeastern US site, Atmos. Chem. Phys., 18, 11471-11491, 10.5194/acp-18-11471-2018, 2018.

Ruan, X., Zhao, C., Zaveri, R. A., He, P., Wang, X., Shao, J., and Geng, L.: Simulations of aerosol pH in China using WRF-Chem (v4.0): sensitivities of aerosol pH and its temporal variations during haze episodes, Geosci. Model Dev., 15, 6143-6164, 10.5194/gmd-15-6143-2022, 2022.

Sharma, B., Jia, S., Polana, A. J., Ahmed, M. S., Haque, R. R., Singh, S., Mao, J., and Sarkar, S.: Seasonal variations in
195   aerosol acidity and its driving factors in the eastern Indo-Gangetic Plain: A quantitative analysis, Chemosphere, 305, 135490, 10.1016/j.chemosphere.2022.135490, 2022.

Shi, G., Xu, J., Peng, X., Xiao, Z., Chen, K., Tian, Y., Guan, X., Feng, Y., Yu, H., Nenes, A., and Russell, A. G.: pH of Aerosols in a Polluted Atmosphere: Source Contributions to Highly Acidic Aerosol, Environ. Sci. Technol., 51, 4289-4296, 10.1021/acs.est.6b05736, 2017.

200 Tao, W., Su, H., Zheng, G., Wang, J., Wei, C., Liu, L., Ma, N., Li, M., Zhang, Q., Pöschl, U., and Cheng, Y.: Aerosol pH and chemical regimes of sulfate formation in aerosol water during winter haze in the North China Plain, Atmos. Chem. Phys., 20, 11729-11746, 10.5194/acp-20-11729-2020, 2020.

van der Werf, G. R., Randerson, J. T., Giglio, L., van Leeuwen, T. T., Chen, Y., Rogers, B. M., Mu, M., van Marle, M. J. E., Morton, D. C., Collatz, G. J., Yokelson, R. J., and Kasibhatla, P. S.: Global fire emissions estimates during 1997–2016,

205 Earth Syst. Sci. Data, 9, 697-720, 10.5194/essd-9-697-2017, 2017.

Vasilakos, P., Russell, A., Weber, R., and Nenes, A.: Understanding nitrate formation in a world with less sulfate, Atmos. Chem. Phys., 18, 12765-12775, 10.5194/acp-18-12765-2018, 2018.

Wang, G., Chen, J., Xu, J., Yun, L., Zhang, M., Li, H., Qin, X., Deng, C., Zheng, H. T., Gui, H., Liu, J., and Huang, K.: Atmospheric Processing at the Sea-Land Interface Over the South China Sea: Secondary Aerosol Formation, Aerosol

210 Acidity, and Role of Sea Salts, J. Geophys. Res.-Atmos, 127, e2021JD036255, 10.1029/2021JD036255, 2022.

Wang, H., Zhang, D., Zhang, Y., Zhai, L., Yin, B., Zhou, F., Geng, Y., Pan, J., Luo, J., Gu, B., and Liu, H.: Ammonia emissions from paddy fields are underestimated in China, Environ. Pollut., 235, 482-488, 10.1016/j.envpol.2017.12.103, 2018.

Wang, H., Li, J., Wu, T., Ma, T., Wei, L. F., Zhang, H., Yang, X., Munger, J. W., Duan, F., Zhang, Y., Feng, Y., Zhang, Q.,

215 Sun, Y., Fu, P. Q., McElroy, M. B., and Song, S.: Model Simulations and Predictions of Hydroxymethanesulfonate (HMS) in the Beijing-Tianjin-Hebei Region, China: Roles of Aqueous Aerosols and Atmospheric Acidity, Environ Sci Technol, 58, 1589-1600, 10.1021/acs.est.3c07306, 2024.

Wang, S., Liu, T., Jang, J., Abbatt, J. P. D., and Chan, A. W. H.: Heterogeneous interactions between SO2 and organic peroxides in submicron aerosol, Atmos. Chem. Phys., 21, 6647-6661, 10.5194/acp-21-6647-2021, 2021.

220 Wang, Y., Zhang, Q., Jiang, J. K., Zhou, W., Wang, B., He, K., Duan, F., Zhang, Q., Philip, S., and Xie, Y.: Enhanced sulfate formation during China's severe winter haze episode in January 2013 missing from current models, J. Geophys Res-Atmos, 119, 10,425-410,440, 10.1002/2013JD021426, 2014.

Wesely, M. L.: Parameterization of surface resistances to gaseous dry deposition in regional-scale numerical models, Atmospheric Environ., 23, 1293-1304, 10.1016/0004-6981(89)90153-4, 1989.

225 Zhang, B., Shen, H., Liu, P., Guo, H., Hu, Y., Chen, Y., Xie, S., Xi, Z., Skipper, T. N., and Russell, A. G.: Significant contrasts in aerosol acidity between China and the United States, Atmos. Chem. Phys., 21, 8341-8356, 10.5194/acp-21-8341-2021, 2021.

Zhang, L., Chen, Y., Zhao, Y., Henze, D. K., Zhu, L., Song, Y., Paulot, F., Liu, X., Pan, Y., Lin, Y., and Huang, B.: Agricultural ammonia emissions in China: reconciling bottom-up and top-down estimates, Atmos. Chem. Phys., 18,

230 339-355, 10.5194/acp-18-339-2018, 2018.

Zheng, B., Tong, D., Li, M., Liu, F., Hong, C. P., Geng, G. N., Li, H. Y., Li, X., Peng, L. Q., Qi, J., Yan, L., Zhang, Y. X., Zhao, H. Y., Zheng, Y. X., He, K. B., and Zhang, Q.: Trends in China's anthropogenic emissions since 2010 as the consequence of clean air actions, Atmos. Chem. Phys., 18, 14095-14111, 10.5194/acp-18-14095-2018, 2018.

Zheng, G., Su, H., Wang, S., Andreae, M., Pöschl, U., and Cheng, Y.: Multiphase buffer theory explains contrasts in

235 atmospheric aerosol acidity, Science, 369, 1374-1377, 10.1126/science.aba3719, 2020.

Zhou, M., Zheng, G., Wang, H., Qiao, L., Zhu, S., Huang, D., An, J., Lou, S., Tao, S., Wang, Q., Yan, R., Ma, Y., Chen, C., Cheng, Y., Su, H., and Huang, C.: Long-term trends and drivers of aerosol pH in eastern China, Atmos. Chem. Phys., 22, 13833-13844, 10.5194/acp-22-13833-2022, 2022.